Hindawi
Security and Communication Networks
Volume 2021, Article ID 1060144, 15 pages
https://doi.org/10.1155/2021/1060144

Research Article

Multitarget Position-Sensitivity Security Transmission with OAM-DM Based on FDA

Changju Zhu, Maozhong Song, Xiaoyu Dang, and Qiuming Zhu

College of Electronic Information Engineering, Nanjing University of Aeronautics and Astronautics, Nanjing 211106, China

Correspondence should be addressed to Maozhong Song; smz108@nuaa.edu.cn

Received 11 June 2021; Revised 5 October 2021; Accepted 30 October 2021; Published 23 November 2021

Academic Editor: Debasis Giri

The multitarget position-sensitivity security transmission scheme with orbital angular momentum (OAM) directional modulation (DM) waveform using the uniform circular frequency diverse array (FDA) is proposed. The transmitter employs FDA to generate dual-mode range-dependent OAM beam pattern, and the direction information of OAM beam is modulated into the signal. According to the modulation method, orthogonal carrier frequency can be designed to realize multitarget position-dependent OAM pattern. In the undesired position, the intensity pattern and the phase front of the radio beam vary randomly with the digital transmission sequence. Because modulation waveform is position-dependent, the technique offers security, as the signal can be purposely distorted in other positions. The composite dual-mode OAM signal makes it more difficult for eavesdroppers to demodulate correct messages. The receiver with a single antenna employs the phase compensation and helical phase factor to restore the correct digital signal in the desired position. Numerical results show that multitarget position-sensitivity OAM-DM technology based on FDA offers the security transmission scheme.

1. Introduction

Wireless communication has the risk of being intercepted without physical-layer security measures [1]. DM technique, which can protect digitally modulated information signals in the prespecified spatial direction to lower the possibility of interception, has been proposed as a promising technique to address physical-layer security communication problems [2, 3]. Most of DM technologies are based on phased array, which generates range-independent steering directions [4, 5]. As compared with phased array, FDA can generate range-dependent beam pattern with a small frequency increment [6–8]. The range-dependent physical-layer security with FDA can be done in several ways [9–18]. The information code can be designed for FDA, which generates the specific radiation pattern. The transmission beam pattern is related to the range and the azimuth angle based on FDA element with the frequency increment for the DM technique, in which the transmitted symbols are purposely distorted to be unrecoverable except for the legitimate user. In [19], 2-bit phase control is used on a two-element FDA antenna, and the generated radiation pattern with direction-dependent projects the phase modulation signal as a constellation for physical-layer security communication. FDA and DM are jointly exploited for point-to-point communication, which provides physical-layer security in both the range and angle dimensions [20]. Reference [21] combines DM technology and artificial noise matrix-aided Costas sequence matrix FDA in precoding systems for multicast communication scenario.

In the field of physical-layer security communication, there are some studies based on OAM for information security. Electromagnetic radiation can carry OAM, and vortex beams of different modes have orthogonality with each other [22–24]. Thus, OAM transmission technique is promising for communication scheme [25, 26]. In the field of quantum and optics, OAM physical-layer security mainly employs the quantum key distribution protocol of entangled photon pairs, hybrid free space optics-THz technology, and OAM multiplexing [27–30]. So far, there are many methods to generate OAM beam [31–36], where the uniform circular array antenna (UCA) has been extensively studied for its

flexibility in generating different OAM modes. In [37], the message is encoded on the OAM mode generated by the uniform circular FDA, and the security with OAM mode modulation is enhanced since the OAM mode can be observed in the desired region only. Due to the direction information carried by OAM beam, it has an application prospect in DM technology for physical-layer security. As compared with traditional DM, it is easier to achieve physical-layer security with the two-dimensional direction. At present, DM mostly focuses on the range and azimuth angle, where the sensitivity needs to be further improved. The vortex beam with two-dimensional direction and range is almost not fully utilized in security communication. OAM beam with range, elevation, and azimuth information, which is generated by FDA, has great potential in multitarget security.

In this paper, the uniform circular FDA element is excited by the designed signal to generate OAM beams related to the range, elevation, and azimuth. The modulated composite OAM-DM signal can be used for security transmission with the space position-sensitivity, and the designed orthogonal carrier frequency can realize multitarget communication. OAM beams generated by the uniform circular FDA with the random frequency offset can maintain the helical phase and the intensity pattern characteristics at the desired range. Then, two-dimensional direction information of OAM beam radiation pattern is modulated into the signal to generate angle-dependent OAM-DM waveform. Because the frequency offset changes randomly with the transmission bit, the intensity pattern and phase front can be randomly distorted in the undesired position without disturbing the desired position. The receiver demodulates dual-mode OAM-DM signal with different modes and synthesizes them, which makes it more difficult for eavesdroppers to demodulate the correct message. Dual-mode OAM-DM signal emphasizes the position-sensitivity for multitarget security transmission and has a low requirement for communication capacity. Moreover, transmitting different modulation constellations in different space positions enables a single antenna receiver to restore the correct digital sequence in the desired position without requiring a larger aperture to receive the whole OAM signal at the farther range, which is different from the traditional OAM signal reception.

Actually, our proposed scheme is different from [37]. Firstly, the FDA generates the range-dependent OAM signal, and the confidential information is encoded on OAM modes in [37]. However, this scheme offers only one-dimensional range-dependent security transmission, which cannot be projected to a specific position in three-dimensional space. Then, the vortex wave is used as a carrier to transmit information, in which the receiver is required to be a large aperture array antenna and aligned with the transmitter for OAM signal reception. Also, the frequency offset increasing regularly makes the wavefront distortion with range exist regularly to a certain extent, in which the signal has the risk of being monitored and restored.

The proposed scheme's major contributions are listed as follows:

(1) We introduce the phase integer ambiguity into the phase excitation of UCA's element, which does not affect the generation of vortex beam. The corresponding relationship between the phase excitation and the frequency offset is designed, which makes the frequency offset change irregularly in FDA. The wavefront with vortex wave characteristics can be generated at the desired range. The wavefront is randomly distorted at the undesired range, which reduces the eavesdropping risk on the wavefront variation law. However, the random frequency offset will not interfere with the vortex wavefront generation at the specific range, which can ensure security transmission at the desired range.

(2) We designed excitation signals for OAM-DM waveform generation in FDA. The range, elevation, and azimuth information carried by dual OAM beams are modulated into the signal constellation to generate OAM-DM signals, which can realize specific position-sensitivity security transmission in three-dimensional space. We design orthogonal carrier frequency for OAM-DM excitation signals to achieve multitarget security communication. The receiver can use a single antenna to demodulate OAM-DM signal related to specific range, elevation, and azimuth at the desired position, without requiring a large aperture array antenna to receive the complete wavefront.

(3) The traditional OAM signal uses a large aperture array antenna to measure the phase gradient at the receiver and requires the receiving array center to be aligned with the beam axis for OAM mode detection. We utilize two OAM-DM signals with different modes to transmit one digital sequence. The single antenna receiver can estimate the OAM mode through the relationship between the two received OAM-DM signals. Digital information in OAM-DM signals can be demodulated by the helix phase factor and compensating phase at the desired position. Further, two OAM-DM signals are synthesized into one signal to restore the correct digital information, which is conducive to reducing the eavesdropping risk.

2. OAM Beams Generated by FDA

2.1. The Uniform Circular Array Antenna. We consider that the OAM beam generation based on UCA is much flexible and easily controlled. M ($M = 8$) antennas in UCA are fed with the phase difference $2\pi l/M$ between each elements, where l denotes the integer OAM mode value and $l < M/2$. In Figure 1(a), UCA can be used to generate OAM beams, where d is the range, δ is the elevation angle, γ is the azimuth angle, and R is the radius of UCA. The helical phase front of OAM beam is shown in Figure 1(b). Each array element is full-wavelength dipole, and the length of each antenna is λ, where λ is the wavelength. In Figure 1(a), all elements in UCA can be excited by s (t) and the phase exp ($jl\beta_m + j\theta$),

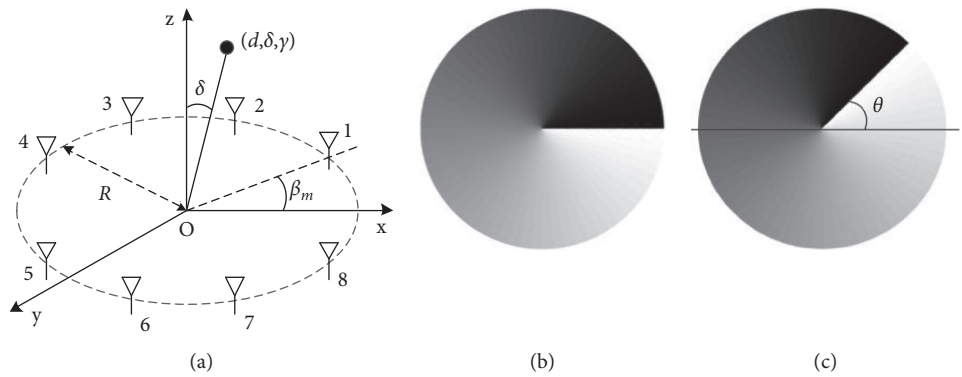

Figure 1: The uniform circular array antenna and the phase front of OAM beam. (a) UCA. (b) The helical phase front of OAM beam. (c) Rotational phase front.

where β_m is the azimuth angle of the mth element, and θ is the rotational phase. The helical phase front will deflect θ integrally in Figure 1(c), which can adjust the azimuth angle.

2.2. Range-Dependent OAM Beam Pattern Generated by the Uniform Circular FDA. For the mth antenna element in Figure 1(a), the radiation frequency can be given by

$$f_{w,m,x} = f_w + \Delta f_{m,x}, \quad x = 1, 2, \tag{1}$$

where f_w denotes the central carrier frequency of wth target, and $\Delta f_{m,x}$ denotes the frequency offset of the mth antenna element. Since the FDA transmission mode is time varying [21, 37], we design the corresponding relationship between frequency offset and phase excitation for mth antenna element at certain time t. For the uniform circular FDA generating OAM beam, the relationship between frequency offset $\Delta f_{m,x}$ and excitation phase $\varphi_{m,x}$ is designed as

$$\begin{aligned}\varphi_{m,x} &= l_x \beta_{m,x} + \theta_x + 2\pi N_x \\ &= 2\pi \Delta f_{m,x}\left(t - \frac{d_0 \cos\ \delta_0}{c}\right) \\ &= 2\pi \Delta f_{m,x}\frac{d_0 \cos\ \delta_0}{c}, \quad \theta_x \in [0, 2\pi],\end{aligned} \tag{2}$$

where d_0 is the desired range, δ_0 is the desired elevation angle, c is the speed of light, t is set to $2d_0\cos\delta_0/c$ and the parameter N_x is an integer randomly generated at certain time t. The azimuth angle $\beta_{m,x}$ of the mth element is expressed as

$$\beta_{m,x} = \frac{2\pi(m-1)}{M}. \tag{3}$$

The phase of each element plus $(\theta_x + 2\pi N_x)$ can make the phase front rotate θ_x without affecting the generation of vortex beam. According to the principle of UCA generating OAM beam, the phase difference between adjacent array elements can be written as

$$\Delta\varphi = \varphi_{m+1,x} - \varphi_{m,x} = \frac{2\pi l}{M}. \tag{4}$$

The phase difference of adjacent array elements is the sum of a fixed value, which satisfies the generation condition of the vortex wave. From equations (2)–(4), the frequency offset $\Delta f_{m,x}$ can be expressed as

$$\Delta f_{m,x} = \frac{2\pi l_x (m-1) + M(\theta_x + 2\pi N_x)}{2\pi M d_0 \cos\ \delta_0} c. \tag{5}$$

The frequency difference between adjacent array elements can be written as

$$\Delta f_{m+1,x} - \Delta f_{m,x} = \frac{l_x c}{M d_0 \cos\ \delta_0}. \tag{6}$$

In FDA-related literature [34], $\Delta f_{m,x}$ is required to satisfy

$$\max\left\{\left|\Delta f_{m,x}\right|\right\} << f_w. \tag{7}$$

The relationship between the frequency offset $\Delta f_{m,x}$ and the integer N_x from equation (5) can be expressed as

$$\begin{aligned}&-\frac{d_0 \cos\ \delta_0 \max\left\{\left|\Delta f_{m,x}\right|\right\}}{c} - \xi \\ &\le N_x \le \frac{d_0 \cos\ \delta_0 \max\left\{\left|\Delta f_{m,x}\right|\right\}}{c} - \xi,\end{aligned} \tag{8}$$

where

$$\xi = \frac{m-1}{M} l + \frac{\theta_x}{2\pi}. \tag{9}$$

The desired range d_0 and the integer N_x can constrain each other. The limited range of the frequency offset $\Delta f_{m,x}$ satisfies $|\Delta f_{m,x}| \le 20$ MHz and c is 3×10^8 m/s. From equation (8), the relationship between N_x and the desired range can be obtained by

$$\begin{cases} \lceil -\dfrac{d_0 \cos\ \delta_0}{15} \rceil \le N_x \le \lfloor \dfrac{d_0 \cos\ \delta_0}{15} - \dfrac{M-1}{M} l - 1 \rfloor, & l > 0, \\ \lceil -\dfrac{d_0 \cos\ \delta_0}{15} - \dfrac{M-1}{M} l \rceil \le N_x \le \lfloor \dfrac{d_0 \cos\ \delta_0}{15} - 1 \rfloor, & l < 0. \end{cases} \tag{10}$$

In equation (10), when $|l| = 1$, 2 and N_x is generated randomly, the frequency offset $|\Delta f_{m,x}|$ is less than 20 MHz at the desired range. As shown in Figure 2, with the increase of the desired range, N_x can take more values randomly. In Figure 3, when $d_0\cos\delta_0 = 60$ m and N_x is generated randomly with the transmission bit, $|\Delta f_{m,x}|$ is always less than 20 MHz. In Figure 4, when $\theta_x = 0$, the minimum desired range is greater than 14 m 13 m, 25 m, and 26 m, respectively, which can ensure that $|\Delta f_{m,x}|$ is always less than 20 MHz. In fact, with the change of θ_x, the minimum desired range has a certain difference. In the uniform circular FDA, the array radius R satisfies

$$R \geq \frac{M \max\{\lambda_{m,x}\}}{4\pi} = \frac{Mc}{4\pi \min\{|f_{w,m,x}|\}}, \tag{11}$$

where $\lambda_{m,x}$ is the wavelength of the beam generated by the mth element. The array radius is affected by the frequency offset. In this paper, R is set to 0.7 max $\{\lambda_{m,x}\}$.

3. OAM-DM Based on FDA

3.1. OAM Signal Design and Direction Modulation. Two excitation signals are designed for the uniform circular FDA. In Figure 1(a), mth element is driven by $s_1(t)$ and $s_2(t)$.

$$\begin{cases} s_1(t) = c_{11}\cos\left[2\pi\left(f_w t + \Delta f_{m,1}\dfrac{d_0\cos\delta_0}{c}\right)\right] + c_{12}\sin\left[2\pi\left(f_w t + \Delta f_{m,1}\dfrac{2d_0\cos\delta_0}{c}\right)\right], \\ s_2(t) = c_{21}\cos\left[2\pi\left(f_w t + \Delta f_{m,2}\dfrac{d_0\cos\delta_0}{c}\right)\right] + c_{22}\sin\left[2\pi\left(f_w t + \Delta f_{m,2}\dfrac{2d_0\cos\delta_0}{c}\right)\right], \end{cases} \tag{12}$$

where c_{ij} is the element of the encoding matrix and $c_{ij} \in [-1, 0, 1]$ $(i, j = 1, 2)$. The radiation pattern of each antenna element in the uniform circular FDA is expressed as

$$\begin{aligned} F(\delta,\gamma) &= \frac{1+\cos(\pi\cos\delta)}{\sin\delta}, \\ \delta &\in \left[0, \frac{\pi}{2}\right], \\ \gamma &\in [0, 2\pi]. \end{aligned} \tag{13}$$

The far-field OAM beam radiation pattern without phase front rotation can be expressed as

$$\begin{aligned} g_x(d,\delta,\gamma,t) &= F(\delta,\gamma)\sum_{m=1}^{M}\exp\left\{j\left[kR\sin\delta\cos(\gamma-\beta_m) + 2\pi\Delta f_{m,x}\left(t - \frac{d\cos\delta}{c}\right) - \theta_x\right]\right\} \\ &= F(\delta,\gamma)\sum_{m=1}^{M}\exp\left\{j\left[kR\sin\delta\cos(\gamma-\beta_m) + 2\pi\Delta f_{m,x}\frac{d\cos\delta}{c} - \theta_x\right]\right\}, \end{aligned} \tag{14}$$

where $k = 2\pi f/c$, $t = 2d_0\cos\delta_0/c$. The complex digital symbol with the magnitude and phase, which can be viewed as a constellation point on the real-imaginary coordinate system, is written as

$$\begin{aligned} E(t) = {} & g_1(d,\delta,\gamma,t)s_1(t)\exp(j\theta_1) \\ & + g_2(d,\delta,\gamma,t)s_2(t)\exp(j\theta_2). \end{aligned} \tag{15}$$

The rotation angle θ_1 is set to 0 as the reference phase. Equation (15) is written as

$$E(t) = a_{1,w}\cos(2\pi f_w t) + a_{2,w}\sin(2\pi f_w t). \tag{16}$$

Equation (16) is written as

$$E(t) = \sqrt{a_{1,w}^2 + a_{2,w}^2}\cos\left(2\pi f_w t - \arctan\frac{a_{1,w}}{a_{2,w}}\right) = B_w\cos(2\pi f_w t - \phi_w). \tag{17}$$

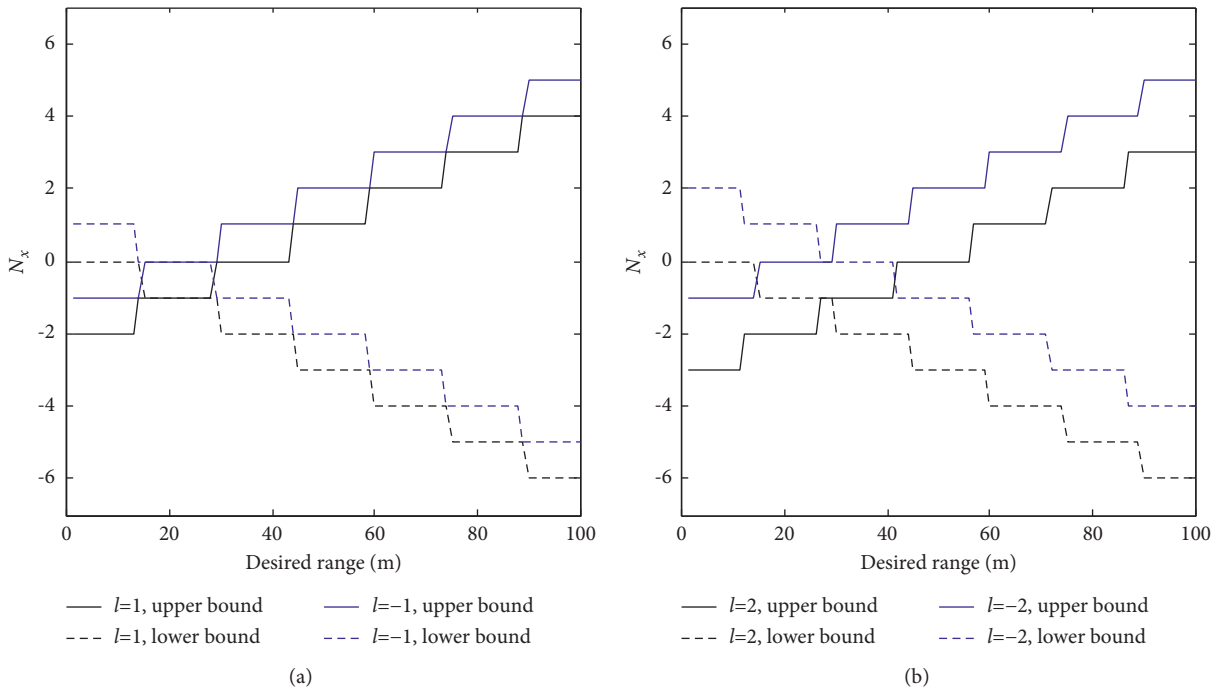

Figure 2: The relationship between the desired range and the range of N_x. (a) Bounds of N_x with $|l| = 1$. (b) Bounds of N_x with $|l| = 2$.

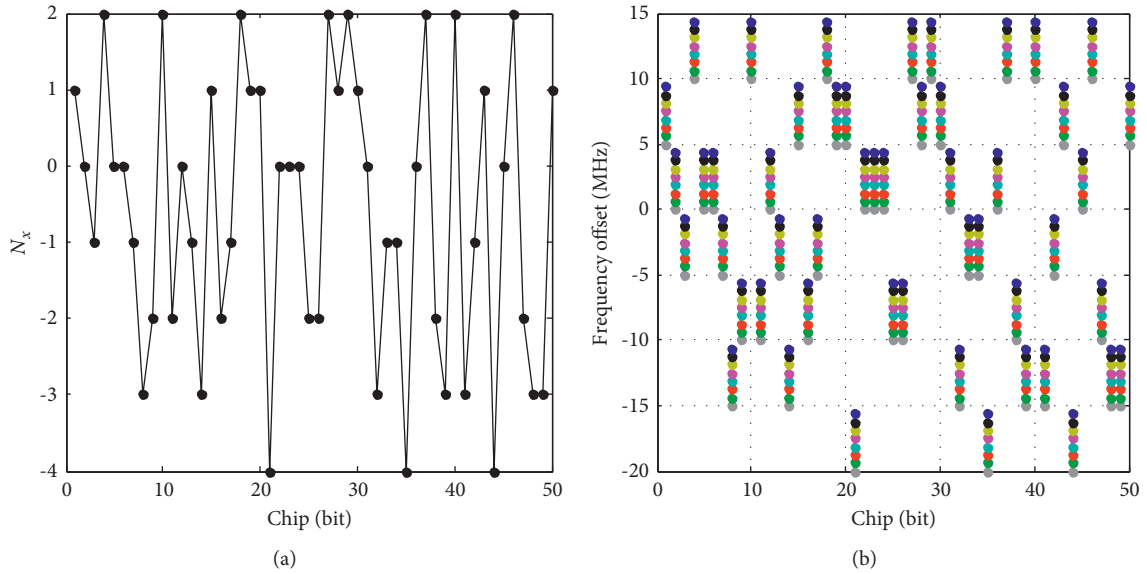

Figure 3: Continued.

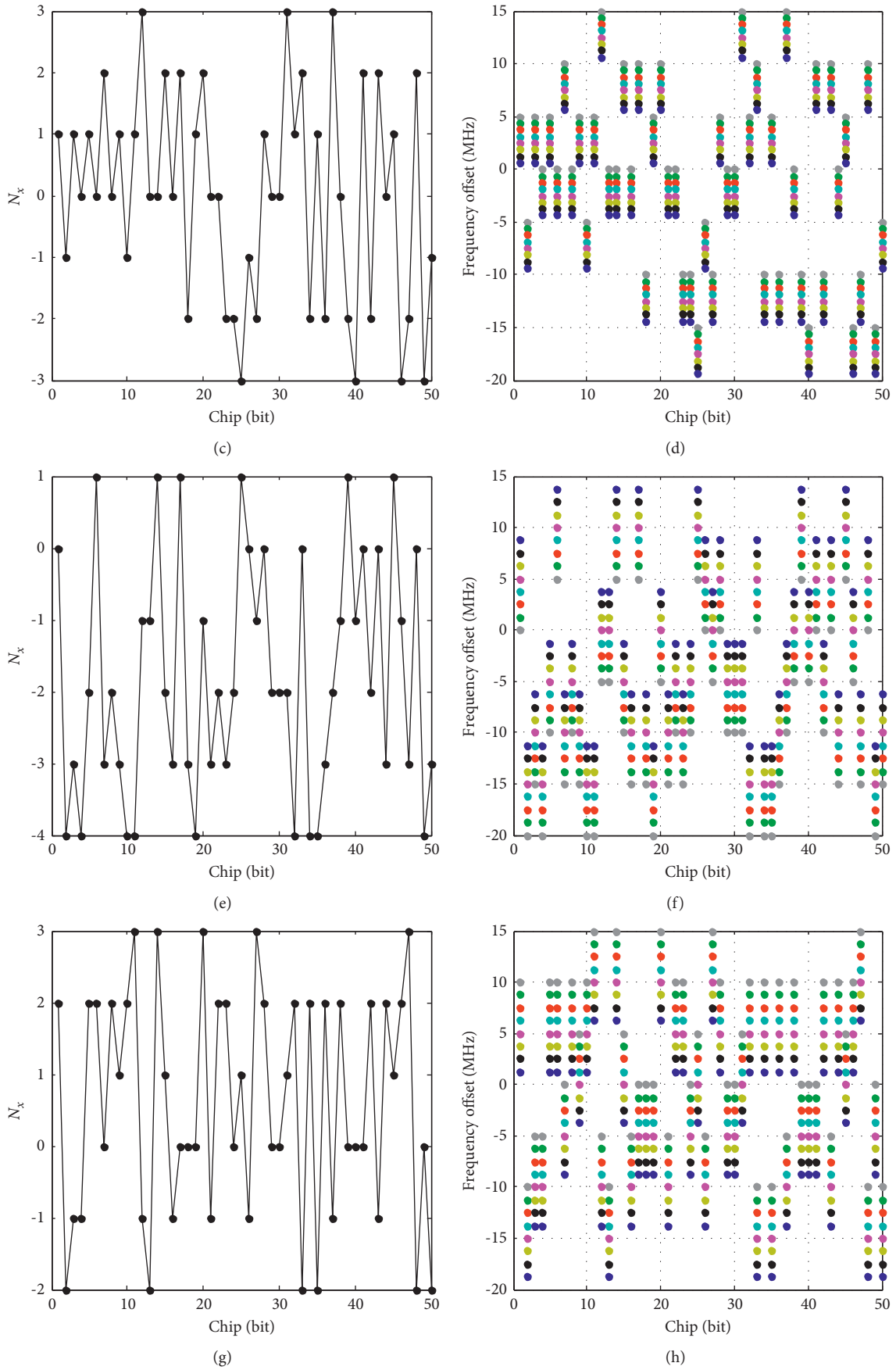

Figure 3: Random N_x and frequency offset of FDA elements in the desired range. (a) Random N_x with $l = 1$. (b) Frequency offset with $l = 1$. (c) Random N_x with $l = -1$. (d) Frequency offset with $l = -1$. (e) Random N_x with $l = 2$. (f) Frequency offset with $l = 2$. (g) Random N_x with $l = -2$. (h) Frequency offset with $l = -2$. A set of points arranged vertically from blue to gray represent the frequency offset of eight elements in (d), (f), and (h).

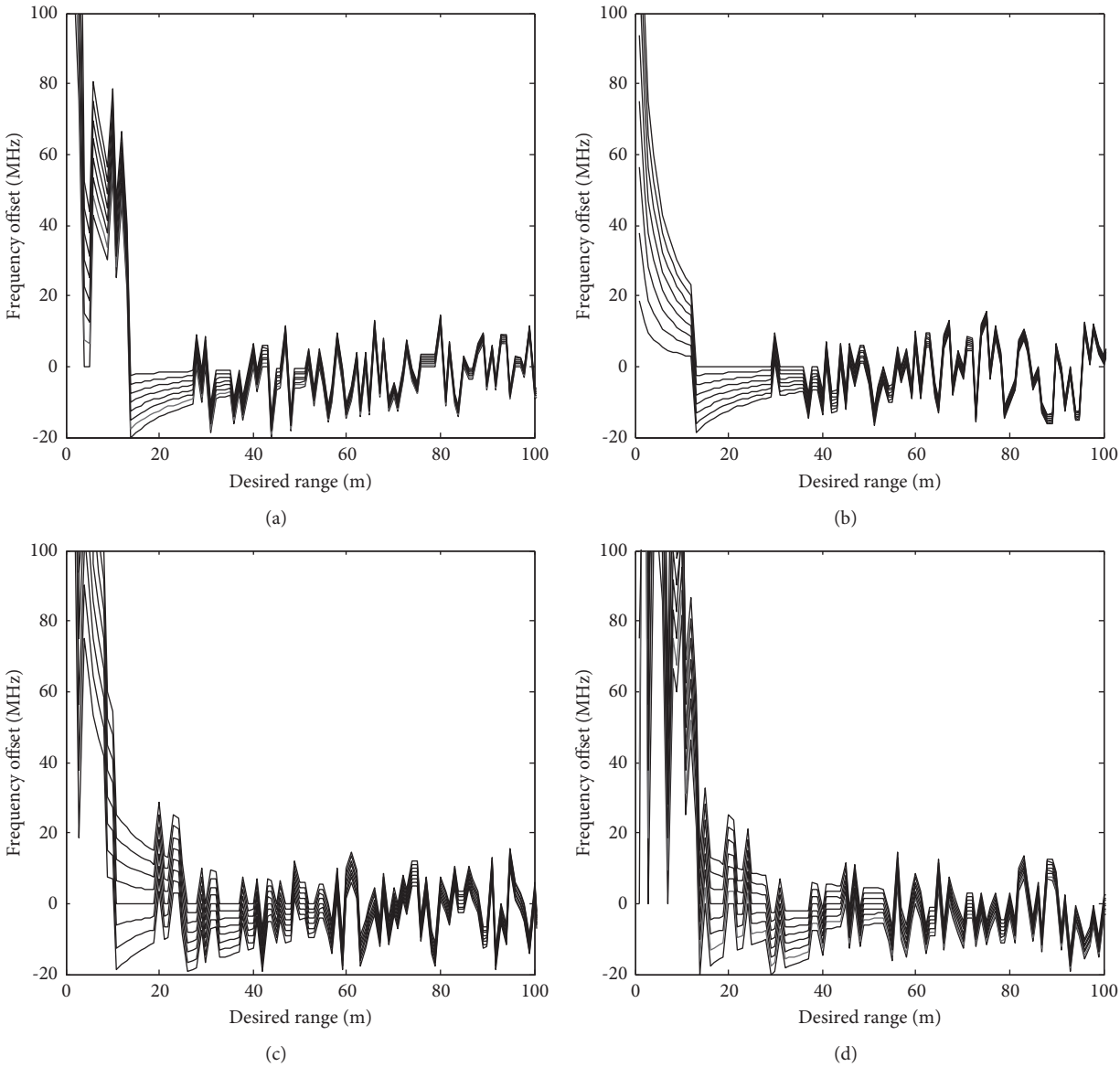

Figure 4: Relationship between the desired range and the frequency offset in FDA. Eight black lines represent frequency offsets of eight elements at the desired range. (a) $l = 1$. (b) $l = -1$. (c) $l = 2$. (d) $l = -2$.

In each bit period $[kT, (k+1)T]$, wth and $(w+1)$th carrier frequencies are designed to be orthogonal, and then

$$\begin{aligned} & B_w B_{w+1} \int_{kT}^{(k+1)T} \cos\left(2\pi f_w t - \phi_w\right) \cos\left(2\pi f_{w+1} t - \phi_{w+1}\right) \mathrm{d}t \\ & = \frac{B_w B_{w+1}}{2} \int_{kT}^{(k+1)T} \cos\left[2\pi\left(f_w + f_{w+1}\right)t - \phi_w - \phi_{w+1}\right] \mathrm{d}t \\ & + \frac{B_w B_{w+1}}{2} \int_{kT}^{(k+1)T} \cos\left[2\pi\left(f_w - f_{w+1}\right)t - \phi_w + \phi_{w+1}\right] \mathrm{d}t. \end{aligned} \tag{18}$$

When $f_{w,m} + f_{w+1,m}$ and $f_{w,m} - f_{w+1,m}$ are integral multiples of $1/T$, the integral result in equation (18) is 0, which can obtain orthogonal OAM signals. Moreover, $f_{w,m} - f_{w+1,m} = 1/T$ is the minimum frequency difference. Thus, multiple orthogonal signals can be generated to realize multitarget communication. The signal on the wth carrier is coded and modulated. From equation (16), the constellation can be expressed as

$$\begin{aligned} a_w &= a_{1,w} + \mathrm{j}a_{2,w} \\ &= [c_{11}\, c_{12}\, c_{21}\, c_{22}]\mathbf{K} + \mathrm{j}[c_{12}\ -c_{11}\, c_{22}\ -c_{21}]\mathbf{K}, \end{aligned} \tag{19}$$

From the modulation matrix **K**, the dual-mode OAM beam pattern with the range, elevation, and azimuth can be modulated into the signal.

$$\mathbf{K} = \begin{bmatrix} g_1(d,\delta,\gamma,t)\cos(\vartheta) \\ g_1(d,\delta,\gamma,t)\sin(\vartheta) \\ g_2(d,\delta,\gamma,t)\cos(\chi) \\ g_2(d,\delta,\gamma,t)\sin(\chi) \end{bmatrix}, \tag{20}$$

where

$$\begin{cases} \chi = 2\pi\Delta f_{m,2}\dfrac{2d_0\cos\delta_0}{c} - \theta_2, \\ \vartheta = 2\pi\Delta f_{m,1}\dfrac{2d_0\cos\delta_0}{c}. \end{cases} \tag{21}$$

3.2. OAM Signal Coding. The digital information can be modulated into the signal by coding the modulation matrix **K**. Designed coding matrix **P** (n) with the data sequence z_n can be given by

$$\mathbf{P} = \mu\mathbf{G}^{\mathrm{T}}\mathbf{H}, \tag{22}$$

where

$$\begin{cases} \mu = \exp\left[j\pi\dfrac{(z_n+1)\mathrm{mod}3}{2}\right], \\ \mathbf{G} = \begin{bmatrix} 0 & 1 & 0 & 0 \\ -1 & 0 & 0 & 0 \\ 0 & 0 & 0 & 1 \\ 0 & 0 & -1 & 0 \end{bmatrix}^{z_n}, \mathrm{H} = \begin{bmatrix} -1 & 0 & 1 & 0 \\ 0 & 1 & 0 & -1 \\ 1 & 0 & 1 & 0 \\ 0 & -1 & 0 & -1 \end{bmatrix}, \end{cases} \tag{23}$$

where $z_n = 0, 1, 2, 3$. Coding matrix **H** is designed for the nth frame and the $(n-1)$th frame signals. The nth frame and the $(n-1)$th frame signals are obtained from

$$[\, a_1(1,n)\ \ a_2(1,n)\ \ a_1(2,n-1)\ \ a_2(2,n-1)\,] = \mathbf{PK}. \tag{24}$$

In equation (24), the dual-mode OAM beam radiation pattern with the position information can be modulated into the signal. Two complex signals (1, n) and a (2, $n-1$) in equation (25) can be obtained.

$$\begin{cases} a(1,n) = a_1(1,n) + ja_2(1,n), \\ a(2,n-1) = a_1(2,n-1) + ja_2(2,n-1). \end{cases} \tag{25}$$

Two frame signals a (1, n) and a (2, $n-1$) are equivalent complex signals, which can generate two QPSK signals. The corresponding relationship between two QPSK signals and data sequence can be given by

$$\begin{aligned} a(1,n) &= \begin{cases} \mu[g_2(d,\delta,\gamma,t)\exp(-j\chi) - g_1(d,\delta,\gamma,t)\exp(-j\vartheta)], & z_n = 0, \\ j\mu[g_2(d,\delta,\gamma,t)\exp(-j\chi) - g_1(d,\delta,\gamma,t)\exp(-j\vartheta)], & z_n = 1, \\ \mu[g_1(d,\delta,\gamma,t)\exp(-j\vartheta) - g_2(d,\delta,\gamma,t)\exp(-j\chi)], & z_n = 2, \\ j\mu[g_1(d,\delta,\gamma,t)\exp(-j\vartheta) - g_2(d,\delta,\gamma,t)\exp(-j\chi)], & z_n = 3, \end{cases} \\ a(2,n-1) &= \begin{cases} \mu[g_2(d,\delta,\gamma,t)\exp(-j\chi) + g_1(d,\delta,\gamma,t)\exp(-j\vartheta)], & z_{n-1} = 0, \\ j\mu[g_2(d,\delta,\gamma,t)\exp(-j\chi) + g_1(d,\delta,\gamma,t)\exp(-j\vartheta)], & z_{n-1} = 1, \\ \mu[-g_1(d,\delta,\gamma,t)\exp(-j\vartheta) - g_2(d,\delta,\gamma,t)\exp(-j\chi)], & z_{n-1} = 2, \\ j\mu[-g_1(d,\delta,\gamma,t)\exp(-j\vartheta) - g_2(d,\delta,\gamma,t)\exp(-j\chi)], & z_{n-1} = 3. \end{cases} \end{aligned} \tag{26}$$

When transmitting sequences z_n and z_{n-1} $(z_n = z_{n-1})$, the receiver synthesizes two QPSK signals into a_{syn} (d, δ, γ, t), which is related to position.

$$a_{\mathrm{syn}}(d,\delta,\gamma,t) = a(1,n) + a(2,n-1). \tag{27}$$

Table 1 shows the receive vectors of the OAM-DM signal, along with the binary bit and created by the four sets of values in the position (d, δ, γ).where

$$a'_{\mathrm{syn}}(d,\delta,\gamma,t) = \frac{a_{\mathrm{syn}}(d,\delta,\gamma,t)}{2\max\left[\left|g_2(d,\delta,\gamma,t)\right|\right]}. \tag{28}$$

According to equation (28), constellation distortion degree of the received signal can be correlated with the elevation angle. At the desired position, constellation phase states of two signals are 0, $\pi/2$, π and $3\pi/2$. Phase states of the synthesized constellation are $\pi/4$, $3\pi/4$, $5\pi/4$ and $7\pi/4$. When N_x is generated randomly with the transmission bit, the phase state is almost stationary at the desired position. In the undesired position, the random N_x can make the signal phase state change irregularly. As shown in Figure 5(a), phase states always remain unchanged at the desired range. However, random N_x can distort phase states of

Table 1: Receive vectors corresponding to different data sets.

Sequence z_n	Binary bit	OAM-DM symbol
0	00	$a'_{syn}(d, \delta, \gamma, t)$
1	10	$ja'_{syn}(d, \delta, \gamma, t)$
2	11	$-a'_{syn}(d, \delta, \gamma, t)$
3	01	$-ja'_{syn}(d, \delta, \gamma, t)$

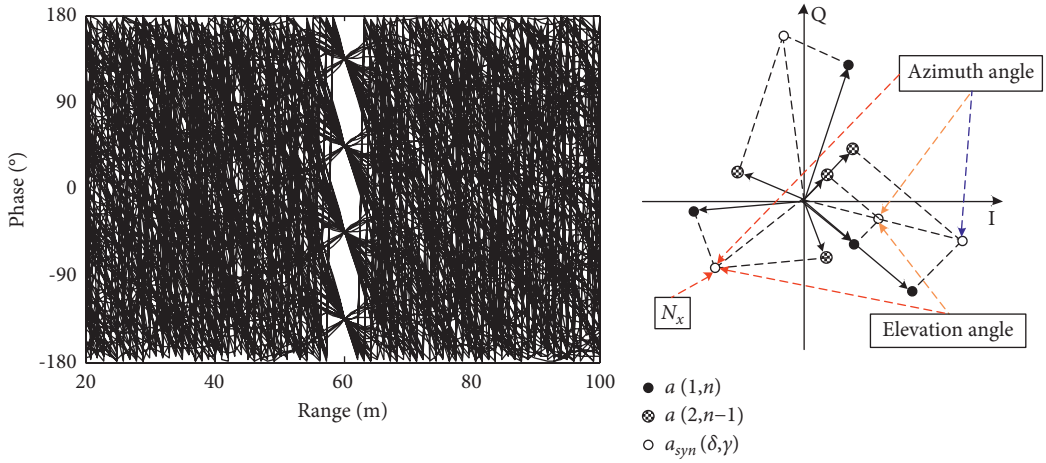

Figure 5: Modulation signal phase state and constellation. (a) Phase state at different ranges. (b) The change of constellation point.

constellation points at other ranges. When the position changes, N_x, elevation and azimuth angle can affect the distortion degree of the constellation. In Figure 5(b), N_x makes the constellation phase state change irregularly at the undesired range, the change of the azimuth angle can make the constellation phase rotation, and the elevation angle can affect the signal amplitude. Due to the position-dependent OAM beam pattern, constellations of two QPSK signals obtained by modulation and code will be distorted to varying degrees in different positions, which can interfere with the eavesdropper to get the correct information. Therefore, dual-mode OAM-DM signal with position-sensitivity can achieve security transmission in the desired position.

When $l_2 = \pm 1$ and $l_1 \neq l_2$, the desired azimuth angle is unique, and OAM beam with mode l_1 can interfere with the eavesdropper to demodulate dual-mode OAM-DM signal. In equation (29), the synthesized signal is related to g_2 and the desired azimuth angle can be adjusted by changing θ_2. Intensity patterns of OAM beams are shown in Figure 6. It is seen that the main beam will broaden as l_x increases, which indicates that the energy diffusion becomes worse with increasing l_x. In this paper, l_x can be set to ± 1, ± 2 and $l_1 \neq l_2$.

4. OAM-DM Signal Reception

When two combined vortex signals are transmitted, it is achieved by multiplying the opposite helical phase factor exp $(-l_x\gamma)$ to receive OAM signals for demodulation [38]. Therefore, OAM mode detection is an important step. One of the challenging problems in OAM communication is the transmission range. When the transmission is farther, the receiving antenna has a larger aperture, which makes it more difficult for the receiver to detect OAM mode at a long distance. In this paper, OAM azimuth information is modulated into the signal, in which the receiver can demodulate correct information with desired azimuth angle. Thus, when the transmission is farther, the single antenna receiver can demodulate OAM signal without a large aperture.

The desired receiver transmits the position ($d_0\cos\delta_0$, δ_0, γ_0) to the transmitter, which can align the desired position of OAM-DM system with the receiver. The receiver can detect the propagation phase $\psi(l_x,\gamma)$ of OAM beam, and the relationship in equation (29) can be obtained.

$$\psi(l_x, \gamma_0) = l_x\gamma_0 + l_x\theta_x. \tag{29}$$

When the transmitter switches OAM mode, θ_x is set to 0. From equation (12), the encoding matrix c_{ij} can be designed as equation (30), and the signal amplitude weighting factor is set to 1 for detecting OAM mode in the desired position.

$$\begin{cases} \begin{bmatrix} c_{11}(n) & c_{12}(n) \\ c_{21}(n) & c_{22}(n) \end{bmatrix} = \begin{bmatrix} 1 & 0 \\ 1 & 0 \end{bmatrix}, & l_x = l_1, \\ \begin{bmatrix} c_{11}(n-1) & c_{12}(n-1) \\ c_{21}(n-1) & c_{22}(n-1) \end{bmatrix} = \begin{bmatrix} 0 & 0 \\ 1 & 0 \end{bmatrix}, & l_x = l_2. \end{cases} \tag{30}$$

For determining the sign of OAM mode value, equation (29) is written as

$$l_x\gamma_0 = \psi(l_x, \gamma_0, n - x + 1). \tag{31}$$

In order to reduce the influence of azimuth angle error on mode detection, equation (31) can be written as

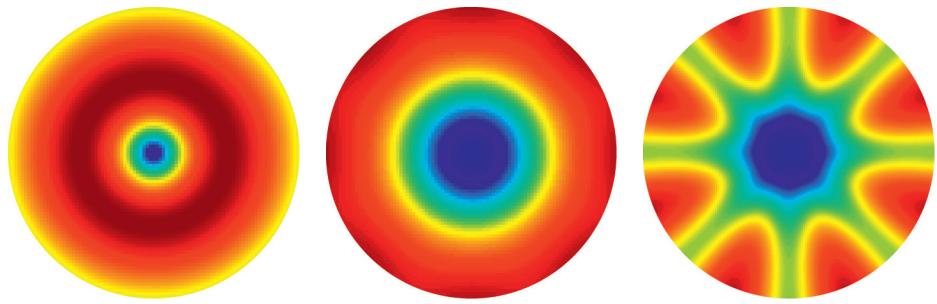

(a) (b) (c)

Figure 6: Intensity patterns. The color changing from blue to green, yellow, and red indicates the increasing intensity of the electric field. (a) $l = \pm 1$. (b) $l = \pm 2$. (c) $l = \pm 3$.

$$Q = \frac{l_1}{l_2} = \frac{\psi(l_1, \gamma_0, n)}{\psi(l_2, \gamma_0, n-1)}, \tag{32}$$

where $l_2 = \pm 1$ and $l_1 \neq l_2$. Thus, l_1 and l_2 can be mapped by OAM mode ratio in Table 2 and equation (31) can be used to judge the sign of the mode value.

When the desired receiver detects OAM mode, the normalized radiation pattern information of OAM beam at ($d\cos\delta$, δ, γ) can be expressed as

$$\begin{aligned} g_x'(d, \delta, \gamma) &= X_x(d, \delta, \gamma) + jY_x(d, \delta, \gamma) \\ &= I_x(\delta)\exp[(j\psi(l_x, \gamma)], \end{aligned} \tag{33}$$

where

$$\begin{cases} I_x = \sqrt{X_x(d, \delta, \gamma)^2 + Y_x(d, \delta, \gamma)^2}, \\ \psi(l_x, \gamma) = \arctan\dfrac{Y_x(d, \delta, \gamma)}{X_x(d, \delta, \gamma)}. \end{cases} \tag{34}$$

In the desired position, equation (33) can maintain the vortex beam characteristic. The vortex signal can be expressed as

$$V_{\text{Mux}}(t) = g_1'(d, \delta, \gamma)s_1(t) + g_2'(d, \delta, \gamma)s_2(t). \tag{35}$$

Table 2: Receive vectors corresponding to different data sets.

Q	(l_1, l_2)
−1	(1, −1) or (−1, 1)
2	(2, 1) or (−2, −1)
−2	(−2, 1) or (2, −1)

From Figure 1(c), θ_x makes the phase front rotate as a whole. Thus, the relationship between compensation azimuth angle γ_1 and θ_x is $l_x\gamma_1 = l_x\theta_x$. Thus, the compensation azimuth angle γ_1 can be expressed as

$$l_x\gamma_1 = \psi(l_x, \gamma) - l_x\gamma. \tag{36}$$

When the receiver is in the desired position ($d_0\cos\delta_0$, δ_0, γ_0), i.e., $d = d_0$, $\delta = \delta_0$ and $\gamma = \gamma_0$, OAM-DM signal can be demodulated by multiplying the helix phase factor exp ($-l_x\gamma_0$) and compensating phase exp ($-l_x\gamma_1$) with a single antenna.

$$V_{\text{Dmux}}(t) = V_{\text{Mux}}(t)\exp[-j(l_x\gamma_0 + \gamma_1)]. \tag{37}$$

Two signals in equation (38) can be obtained by demodulating the signals with l_1 and l_2, respectively.

$$V_{\text{Dmux}}(t) = \begin{cases} I_1 s_1(t)\exp[jl_1(\gamma - \gamma_0)] + I_2 s_2(t)\exp\{j[\psi_1(l_2, \gamma) - \psi_1(l_1, \gamma) + l_1(\gamma - \gamma_0)]\}, & l_x = l_1, \\ I_2 s_2(t)\exp[jl_2(\gamma - \gamma_0)] + I_1 s_1(t)\exp\{j[\psi_1(l_1, \gamma) - \psi_1(l_2, \gamma) + l_2(\gamma - \gamma_0)]\}, & l_x = l_2. \end{cases} \tag{38}$$

Two frame signals can be demodulated from equation (38) and synthesized into the QPSK signal V_{QPSK} for eliminating the influence of θ_x on the signal demodulation.

$$V_{\text{QPSK}} = \begin{cases} 2I_2(\delta)\exp[jl_2(\gamma - \gamma_0)], & z_n' = 0, \\ 2jI_2(\delta)\exp[jl_2(\gamma - \gamma_0)], & z_n' = 1, \\ -2I_2(\delta)\exp[jl_2(\gamma - \gamma_0)], & z_n' = 2, \\ -2jI_2(\delta)\exp[jl_2(\gamma - \gamma_0)], & z_n' = 3. \end{cases} \tag{39}$$

In the desired position ($d = d_0$, $\delta = \delta_0$ and $\gamma = \gamma_0$), the desired receiver can restore correct signal constellation with $l_x = l_2$. The data sequence can be calculated by the traditional QPSK signal demodulation method.

$$\exp\left(j\frac{\pi z_n'}{2}\right) = V_{\text{QPSK}}\exp[jl_2(\gamma_0 - \gamma)]. \tag{40}$$

Since equation (22) disturbs the distribution of the digital sequence from equation (40) is not the correct data sequence.

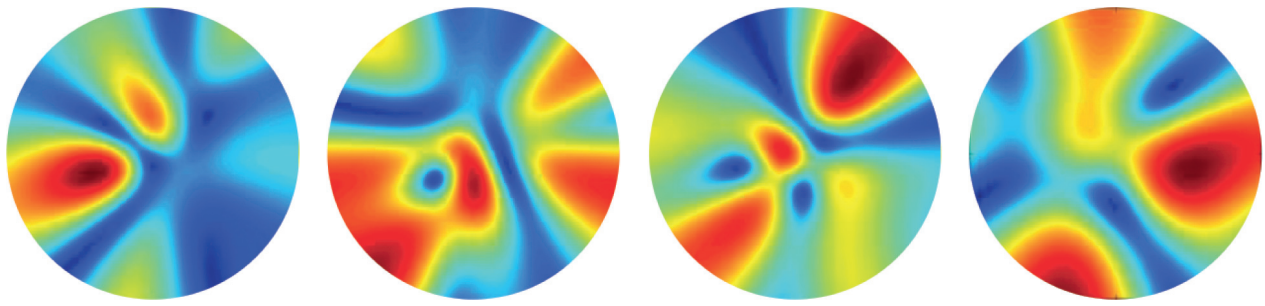

(a) (b) (c) (d)

FIGURE 7: Intensity patterns. The desired range is d_0, $d \neq d_0$. (a) $|l| = 1$. (b) $|l| = 1$, random N_x. (c) $|l| = 2$. (d) $|l| = 2$, random N_x. The color changing from blue to green, yellow, and red indicates an increasing intensity of the electric field.

The constellation needs the specific phase rotation to demodulate the original digital sequence z_n. The correct digital sequence z_n can be obtained by

$$\exp\left(j\frac{\pi z_n}{2}\right) = \exp\left\{j\pi\left[\frac{z_n'}{2} + \frac{(z_n'+4)(z_n'+3)-6}{4}\right]\right\}. \tag{41}$$

Moreover, when the receiver is located at the desired elevation angle δ_0, the signal amplitude $2I_2$ is the largest, and the bit error rate (BER) performance will be the best. The composite mode of OAM-DM signal and the changing OAM mode can make it more difficult for the eavesdropper to demodulate OAM-DM signals. The desired receiver can estimate the OAM mode using the azimuth angle relative to the transmitter, which enables the single antenna receiver to demodulate dual-mode OAM-DM signal. When two signals are synthesized into one signal, the receiver uses the special demodulation method to restore the correct digital information in the desired position.

Since the wave propagates with time, the beam cannot dwell for a long time. This implies that the eavesdropper can receive the same signal as the legitimate user, when they are both in the same position. From our design of OAM-DM signal in random FDA, the signal demodulation depends on OAM mode value, and the transmitter can flexibly switch OAM modes to interfere with eavesdropping. However, OAM-DM signal generated by the random frequency causes OAM mode value to be detected only at the desired range. The eavesdropper must accurately obtain the desired range before it is possible to monitor modes of randomly varying dual OAM beams. Even if the eavesdropper can obtain OAM mode value at the desired range, it must be located at the desired elevation and azimuth to restore correctly two OAM-DM signal constellations. In other words, the eavesdropper must exactly be consistent with the spatial coordinates of the desired receiver to restore the desired signal constellation with correct information, which is extremely difficult for the eavesdropper.

5. Numerical Results

In numerical simulation, BER is calculated by transmitting a data stream of random QPSK symbols in an additive white Gaussian noise (AWGN) channel. Calculating BER via the data stream approach makes Gray-code inspection for each symbol pair possible. When $l_2 = \pm 1$ and $l_1 \neq l_2$, a data stream with 10^6 random QPSK symbols can be used for the BER simulation. Intensity patterns, phase fronts, and multitarget BER performances of the position-sensitivity OAM-DM signal are evaluated.

The desired position ($d_0\cos\delta_0$, δ_0, γ_0) is set to (60 m, 20°, 40°). In Figures 6(a) and 6(b), the intensity pattern of the radio wave is depicted at the desired range, which is not affected by N_x. When the receiver is located at the undesired range, intensity patterns are shown in Figure 7. As shown in Figures 6(a), 6(b), and 7, the intensity pattern only keeps characteristic of vortex wave at the desired range, while intensity patterns at other ranges are distorted randomly with random N_x. Figure 8 depicts phase fronts at different ranges. In Figures 8(a) and 8(c), the vortex phase front of the electric field can be easily recognized at the desired range, for both $l = 1$ and $l = 2$. When $l = -1$ and $l = -2$, the color changing from red to yellow, green, and blue back to red again indicates the phases changing from 0 to 2π. In Figures 8(b) and 8(d), it shows that the field obtained at the undesired range does not exhibit the helical phase fronts. In the desired position, the helical phases of OAM beam with positive and negative mode values are opposite, and elevation information of the radiation pattern is the same. The change of the OAM mode value is used to interfere with the eavesdropper to obtain the correct information without affecting the desired receiver to demodulate the digital information.

Multitarget desired positions are set to (50 m, 20°, 150°), (60 m, 20°, 40°), and (70 m, 20°, 120°), respectively. The mode of dual OAM-DM beams is set to $l_1 = 2$ and $l_2 = 1$. The signal-noise ratio (SNR) is 12 dB. As shown in Figure 9, BER performances with the position-sensitivity OAM-DM signal are simulated. The BER performance is the best in the desired position and varies with the change of the position. Numerical results in Figures 9(a), 9(b), and 9(c) show that the proposed communication scheme with the position-sensitivity OAM-DM pattern can generate a secure position in free space for the desired receiver without knowledge of the eavesdropper's channel state information. Figure 9(d) shows BER performance of the desired receiver under different SNRs and positions. When the position of

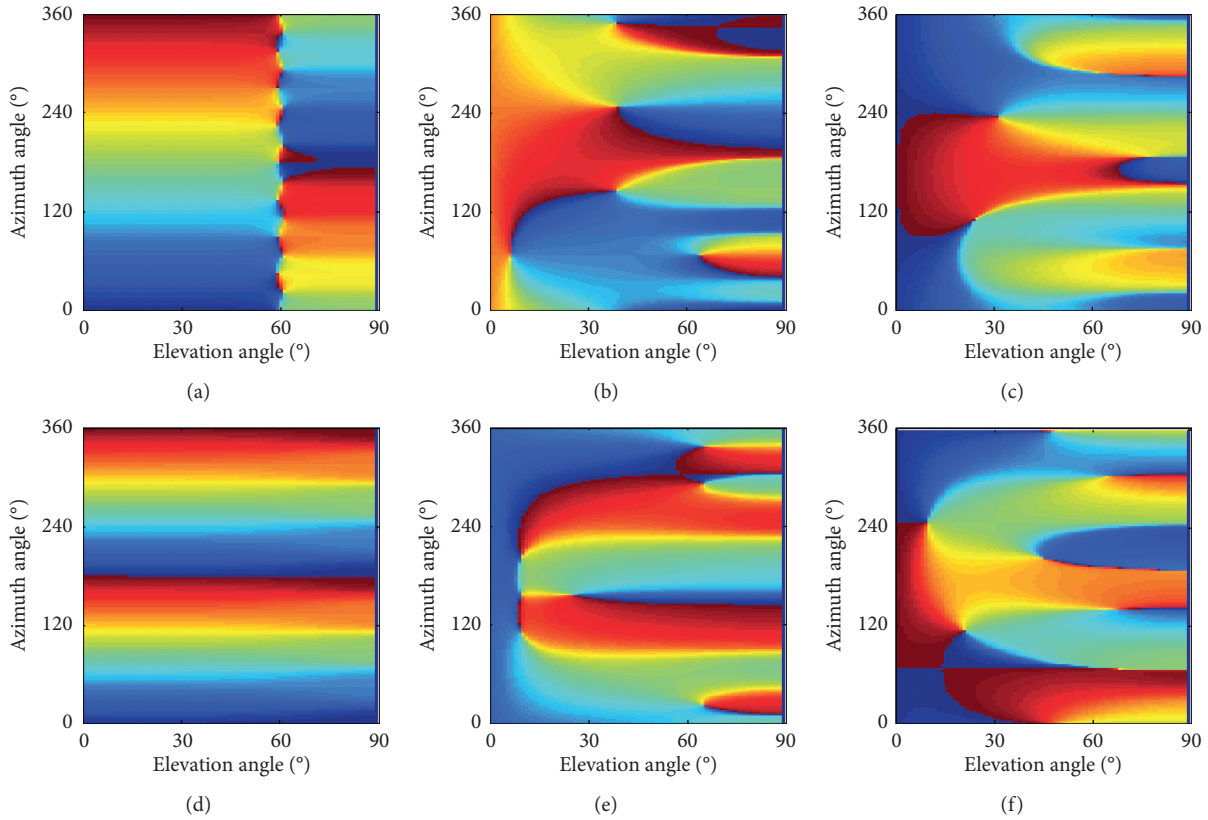

Figure 8: Phase fronts. The desired range is d_0, (a) $d = d_0$, $l = 1$. (b) $d \neq d_0$, $l = 1$. (c) $d \neq d_0$, $l = 1$, random N_x. (d) $d = d_0$, $l = 2$. (e) $d \neq d_0$, $l = 2$. (f) $d \neq d_0$, $l = 2$, random N_x. The color changing from blue to green, yellow, and red back to blue again indicates the phases changing from 0 to 2π.

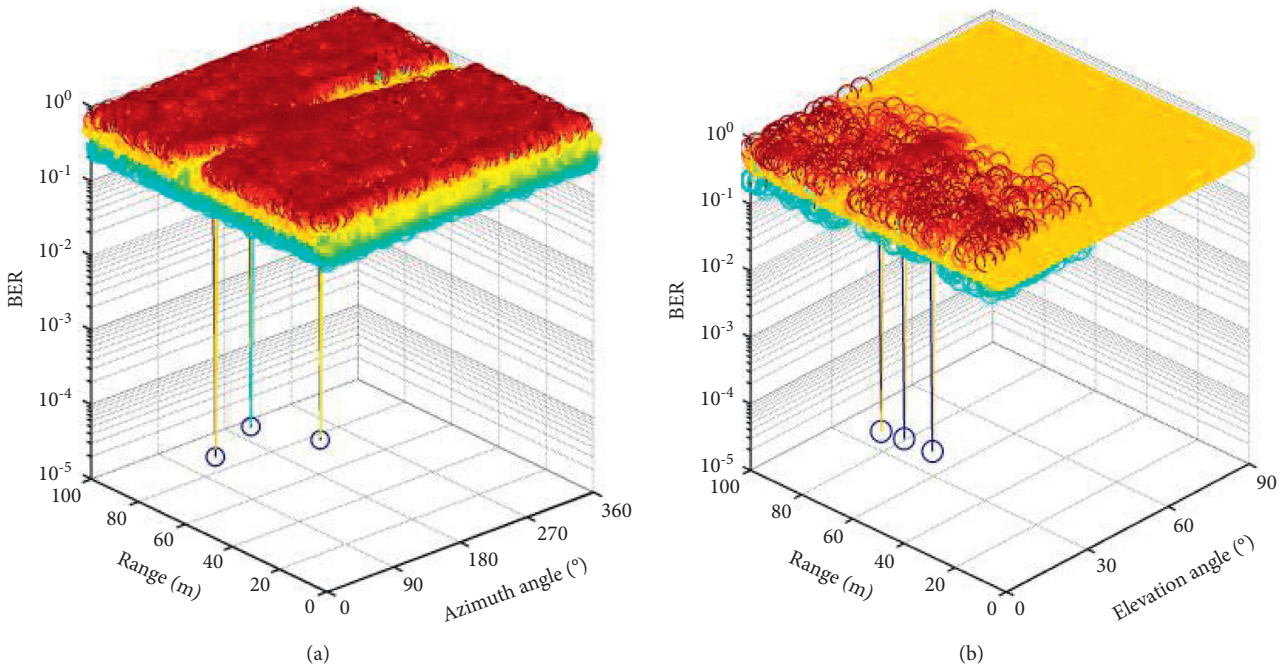

Figure 9: Continued.

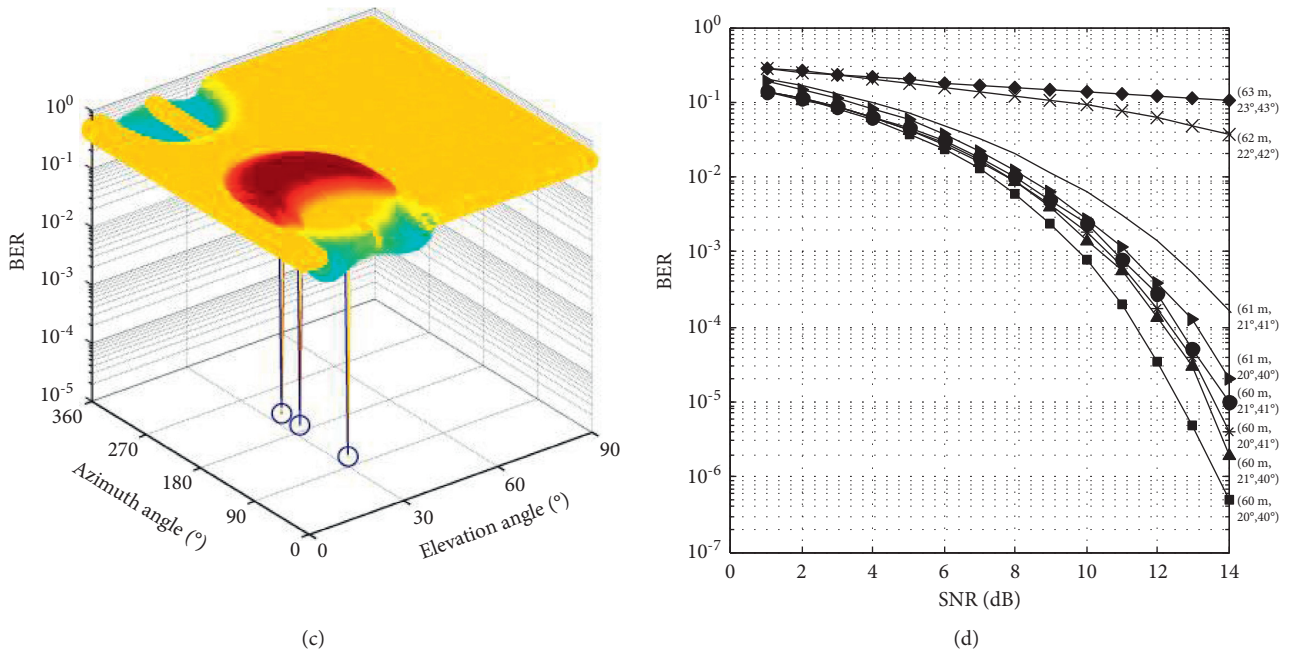

(c) (d)

Figure 9: The BER performance. Multitarget desired positions ($d_0\cos\delta_0$, δ_0, γ_0) are (50 m, 20°, 150°), (60 m, 20°, 40°), and (70 m, 20°, 120°), respectively. (a) The BER performance in desired range and azimuth angle. (b) The BER performance in desired range and elevation angle. (c) The BER performance in desired azimuth and elevation angles. (d) The BER performance under different SNRs.

the desired receiver deviates from the desired position by 1 m and 1°, the BER performance reduces to a certain extent. If the position of the desired receiver deviates from the desired position by more than 1 m and 1°, the BER performance decreases sharply. Even if eavesdroppers have the ability to demodulate signals, it is difficult to obtain the accurate desired position. Therefore, the position-sensitivity OAM-DM signal can still protect multitarget information security.

6. Conclusions

In this study, OAM-DM signal design based on the uniform circular FDA and vortex signal demodulation schemes are proposed for multitarget position-dependent security transmission. The radiation pattern is modulated into the signal, which makes the modulated waveform carry range, elevation, and azimuth information to distort the constellation in all directions except that of the desired position. The eavesdropper outside the desired range observes distorted intensity patterns, phase fronts, and modulation constellation. The phase and amplitude of the constellation point are distorted at the undesired elevation and azimuth angle. Therefore, OAM-DM signal can correlate the position-sensitivity security transmission, in which the eavesdropper cannot recover OAM beam and messages. Moreover, composite signals with dual-mode OAM-DM beam can make it more difficult for eavesdroppers to demodulate OAM-DM signal. OAM mode estimation and the phase compensation enable multiple desired receivers to demodulate OAM-DM signal with a single antenna in the corresponding desired position.

Data Availability

The data used to support the findings of this study are available from the corresponding author upon request.

Conflicts of Interest

The authors declare that there are no conflicts of interest regarding the publication of this article.

Acknowledgments

This is work was supported in part by the National Natural Science Foundation of China (grant no. 62031017) and Aeronautical Science Foundation of China (grant no. 20190105200).

References

[1] Y. Liu, H. H. Chen, and L. Wang, "Physical layer security for next generation wireless networks: theories, technologies, and challenges," *IEEE Communications Surveys & Tutorials*, vol. 19, no. 1, pp. 347–376, 2017.

[2] X. Sun, D. W. K. Ng, Z. Ding, Y. Xu, and Z. Zhong, "Physical layer security in UAV systems: challenges and opportunities," *IEEE Wireless Communications*, vol. 26, no. 5, pp. 40–47, 2019.

[3] Z. Bo and W. Liu, "Multi-carrier based phased antenna array design for directional modulation," *IET Microwaves, Antennas & Propagation*, vol. 12, no. 5, pp. 765–772, 2017.

[4] Z. Spasojevic, S. Dedeo, and R. Jensen, "Dwell scheduling algorithms for phased array antenna," *IEEE Transactions on Aerospace and Electronic Systems*, vol. 49, no. 1, pp. 42–54, 2013.

[5] W. Q. Wang, "Frequency diverse array antenna: new opportunities," *IEEE Antennas and Propagation Magazine*, vol. 57, no. 2, pp. 145–152, 2015.

[6] J. Gao, Z. Yuan, B. Qiu, and J. Zhou, "Secure multiusers directional modulation scheme based on random frequency diverse arrays in broadcasting systems," *Security and Communication Networks*, vol. 2020, Article ID 419859, 11 pages, 2020.

[7] H. Shao, J. Cai, and W. Q. Wang, "Decoupled frequency diverse array range–angle-dependent beampattern synthesis using non-linearly increasing frequency offsets," *IET Microwaves, Antennas & Propagation*, vol. 10, no. 8, pp. 880–884, 2016.

[8] S. Y. Nusenu, W. Q. Wang, and J. Xiong, "Time-modulated FDA for physical-layer security," *IET Microwaves, Antennas & Propagation*, vol. 11, no. 9, pp. 1274–1279, 2017.

[9] W. Q. Wang, "DM using FDA antenna for secure transmission," *IET Microwaves, Antennas & Propagation*, vol. 11, no. 3, pp. 336–345, 2017.

[10] Q. Cheng, V. Fusco, J. Zhu, S. Wang, and F. Wang, "WFRFT-aided Power-efficient Multi-beam directional modulation schemes based on frequency diverse array," *IEEE Transactions on Wireless Communications*, vol. 18, no. 11, pp. 5211–5226, 2019.

[11] J. Gao, B. Qiu, and J. Zhou, "Spatial Modulation and MP-WFRFT-Aided Multi-beam wireless communication scheme based on random frequency diverse array," *Sensors*, vol. 20, no. 18, p. 5289, 2020.

[12] S. Wang, S. Yan, J. Zhang, N. Yang, R. Chen, and F. Shu, "Secrecy zone achieved by directional modulation with random frequency diverse array," *IEEE Transactions on Vehicular Technology*, vol. 70, no. 2, pp. 2001–2006, 2021.

[13] J. Xie, B. Qiu, Q. Wang, and J. Qu, "Broadcasting directional modulation based on random frequency diverse array," *Wireless Communications and Mobile Computing*, vol. 2019, Article ID 5051490, 12 pages, 2019.

[14] S. Y. Nusenu, S. Huaizong, Y. Pan, and A. Basit, "Directional modulation with precise legitimate location using time-modulation retrodirective frequency diversity array for secure IoT communications," *IEEE Systems Journal*, vol. 15, no. 1, pp. 1109–1119, 2020.

[15] Y. Ding, J. Zhang, and V. Fusco, "Frequency diverse array OFDM transmitter for secure wireless communication," *Electronics Letters*, vol. 51, no. 17, pp. 1374–1376, 2015.

[16] N. S. Yaw and W. Wang, "Range-dependent spatial modulation using frequency diverse array for OFDM wireless communications," *IEEE Transactions on Vehicular Technology*, vol. 67, no. 11, pp. 10886–10895, 2018.

[17] J. Gao, Z. Yuan, J. Zhou, and B. Qiu, "Artificial-noise-aided energy-efficient secure multibeam wireless communication schemes based on frequency diverse array," *Wireless Communications and Mobile Computing*, vol. 2020, Article ID 4715929, 14 pages, 2020.

[18] B. Qiu, L. Wang, J. Xie, Z. Zhang, Y. Wang, and M. Tao, "Multi-beam index modulation with cooperative legitimate users schemes based on frequency diverse array," *IEEE Transactions on Vehicular Technology*, vol. 69, no. 10, pp. 11028–11041, 2020.

[19] S. Y. Nusenu, W. Q. Wang, and S. Ji, "Secure directional modulation using frequency diverse array antenna," *Proceedings of the IEEE Radar Conference*, pp. 8–12, 2017.

[20] J. Xiong, S. Y. Nusenu, and W. Q. Wang, "Directional modulation using frequency diverse array for secure communications," *Wireless Personal Communications*, vol. 95, no. 3, pp. 2679–2689, 2017.

[21] S. Y. Nusenu, "Authentication and secrecy of multi-cast communication scenario: artificial noise-aided Costas sequence matrix FDA approach," *Security and Communication Networks*, vol. 2020, Article ID 2194840, 13 pages, 2020.

[22] R. M. Fouda, T. C. Baum, and K. Ghorbani, "Quasi-orbital angular momentum (Q-OAM) generated by quasi-circular array antenna (QCA)," *Scientific Reports*, vol. 8, no. 1, p. 8363, 2018.

[23] Z. Wang, N. Zhang, and X. C. Yuan, "High-volume optical vortex multiplexing and de-multiplexing for free-space optical communication," *Optics Express*, vol. 19, no. 2, pp. 482–492, 2011.

[24] P. Yang, Y. Xiao, M. Xiao, and S. Li, "6G wireless communications: vision and potential techniques," *IEEE Network*, vol. 33, no. 4, pp. 70–75, 2019.

[25] S. Zhao, L. Gong, Y. Li et al., "A Large-alphabet quantum key distribution protocol using orbital angular momentum entanglement," *Chinese Physics Letters*, vol. 30, no. 6, pp. 305–343, 2013.

[26] L. Zhao, H. Liu, Y. Hao, H. Sun, and Z. Wei, "Effects of atmospheric turbulence on OAM-POL-FDM hybrid multiplexing communication system," *Applied Sciences*, vol. 9, no. 23, p. 5063, 2019.

[27] I. B. Djordjevic, "OAM-based hybrid free-space optical-terahertz multidimensional coded modulation and physical-layer security," *IEEE Photonics Journal*, vol. 9, no. 4, Article ID 7905812, 2017.

[28] X. Sun and I. B. Djordjevic, "Physical-layer security in orbital angular momentum multiplexing free-space optical communications," *IEEE Photonics Journal*, vol. 8, no. 1, Article ID 7901110, 2016.

[29] T. Wang, J. Gariano, and I. B. Djordjevic, "Employing Bessel-Gaussian beams to improve physical-layer security in free-space optical communications," *IEEE Photonics Journal*, vol. 10, no. 5, Article ID 7907113, 2018.

[30] T. Wang and I. B. Djordjevic, "Physical-layer security of a binary data sequence transmitted with Bessel-Gaussian beams over an optical wiretap channel," *IEEE Photonics Journal*, vol. 10, no. 6, Article ID 7908611, 2018.

[31] G.-T. Chen, Y.-C. Jiao, and G. Zhao, "A reflectarray for generating wideband circularly polarized orbital angular momentum vortex wave," *IEEE Antennas and Wireless Propagation Letters*, vol. 18, no. 1, pp. 182–186, 2019.

[32] C. Zhang and L. Ma, "Millimetre wave with rotational orbital angular momentum," *Scientific Reports*, vol. 6, no. 1, p. 31921, 2016.

[33] F. Shen, J. Mu, K. Guo, S. Wang, and Z. Guo, "Generation of continuously variable-mode vortex electromagnetic waves with three-dimensional helical antenna," *IEEE Antennas and Wireless Propagation Letters*, vol. 18, no. 6, pp. 1091–1095, 2019.

[34] L. Cheng, W. Hong, and Z. C. Hao, "Generation of electromagnetic waves with arbitrary orbital angular momentum modes," *Scientific Reports*, vol. 4, no. 1, p. 4814, 2014.

[35] S. M. Mohammadi, L. K. S. Daldorff, J. E. S. Bergman et al., "Orbital angular momentum in radio-a system study," *IEEE Transactions on Antennas and Propagation*, vol. 58, no. 2, pp. 565–572, 2010.

[36] F. Zheng, Y. Chen, S. Ji, and G. Duan, "Research status and prospects of orbital angular momentum technology in wireless communication," *Progress in Electromagnetics Research*, vol. 168, pp. 113–132, 2020.

[37] J. Luo, S. Wang, and F. Wang, "Secure range-dependent transmission with orbital angular momentum," *IEEE Communications Letters*, vol. 23, no. 7, pp. 1178–1181, 2019.

[38] Q. Zhu, T. Jiang, Y. Cao, K. Luo, and N. Zhou, "Radio vortex for future wireless broadband communications with high capacity," *IEEE Wireless Communications*, vol. 22, no. 6, pp. 98–104, 2015.